Measurement of tensor analyzing powers in deuteron photodisintegration.

I.A.Rachek,[1] L.M.Barkov,[1] S.L.Belostotsky,[2] V.F.Dmitriev,[1] M.V.Dyug,[1] R.Gilman,[3] R.J. Holt,[4] B.A.Lazarenko,[1] S.I.Mishnev,[1] V.V.Nelyubin,[2] D.M.Nikolenko,[1] A.V.Osipov,[5] D.H. Potterveld,[4] R.Sh.Sadykov,[1] Yu.V.Shestakov,[1] V.N.Stibunov,[5] D.K.Toporkov,[1] H.de Vries,[6] and S.A.Zevakov[1]

[1]*Budker Institute of Nuclear Physics, 630090 Novosibirsk, Russia*
[2]*Saint-Petersburg Institute of Nuclear Physics, 188350 Gatchina, Russia*
[3]*Rutgers University, Piscataway, NJ 08855, USA*
[4]*Argonne National Laboratory, Argonne, IL 60439, USA*
[5]*Institute of Nuclear Physics at Tomsk Polytechnic University, 634050 Tomsk, Russia*
[6]*NIKHEF, P.O.Box 41882, 1009 DB Amsterdam, The Netherlands*

(Dated: November 17, 2006)

A new accurate measurement of the tensor analyzing powers T_{20}, T_{21} and T_{22} in deuteron photodisintegration has been performed. Wide-aperture non-magnetic detectors allowed broad kinematic coverage in a single setup: E_γ = 25 to 600 MeV, and θ_p^{cm} = 24° to 48° and 70° to 102°. The new data provide a significant improvement over the few existing measurements. The angular dependency of the tensor asymmetries in deuteron photodisintegration is extracted for the first time.

PACS numbers: 24.70.+s, 24.20.-x

The simplest nucleus, the deuteron, is a natural laboratory for the study of nuclear forces. One of the most fundamental processes on the deuteron is two-body photodisintegration $\gamma + \mathrm{d} \to p + n$. It has been a subject of intensive experimental and theoretical research for over 70 years (see Ref. [1] for a comprehensive review). However several important observables still are measured with insufficient accuracy or not measured at all. The tensor analyzing powers accessible through measurement of target asymmetries in photodisintegration of tensor polarized deuteron are among the most poorly known. Polarization observables are expected to be sensitive to important dynamical details and thus allow in general much more stringent tests of theoretical models. The tensor polarizations are especially interesting because there is a correlation between the degree of tensor polarization and the spatial alignment of the deuteron. For example, spatial alignment of the target deuterons can lead to large asymmetries from final state interactions in photodisintegration.

A general expression for the cross-section of the two-body photodisintegration of the polarized deuteron is written as follows:

$$\begin{aligned}\frac{d\sigma}{d\Omega} = \frac{d\sigma_0}{d\Omega}\Big\{1 - \sqrt{3/4}\,P_z \sin\theta_H \sin\phi_H\, \mathrm{T}_{11} \\ + \sqrt{1/2}P_{zz}\big[(3/2\cos^2\theta_H - 1/2)\mathrm{T}_{20} \\ - \sqrt{3/8}\sin 2\theta_H\, \cos\phi_H\, \mathrm{T}_{21} \\ + \sqrt{3/8}\sin^2\theta_H\, \cos 2\phi_H\, \mathrm{T}_{22}\big]\Big\},\end{aligned} \tag{1}$$

with σ_0 the unpolarized cross-section, P_z (P_{zz}) the degree of vector (tensor) polarization of the target, θ_H the angle between polarization axis and momentum of γ-quantum, and ϕ_H the angle between the polarization plane (containing the polarization axis and momentum of the photon) and the reaction plane (containing momenta of the proton and neutron). The tensor analyzing powers T_{2I} are functions of photon energy E_γ and proton emission angle θ_p^{cm}.

Only three measurements of tensor polarization observables in deuteron photodisintegration have been reported prior to this experiment. The first experiment was carried out at VEPP–2. The T_{21} component was measured using an internal gas target [2]. In [3], completed at the Bonn Synchrotron using a polarized solid target, a tensor target asymmetry was evaluated for one kinematic point. Finally, at VEPP–3 the components T_{20} and T_{22} were measured in an internal target experiment that simultaneously studied elastic electron-deuteron scattering [4]. Here we present the results of a new measurement of the tensor analyzing power components T_{20}, T_{21} and T_{22}.

The measurements were performed at the 2 GeV electron storage ring VEPP–3. A thin-wall open-ended storage cell fed by polarized deuterium gas from an atomic beam source was used as an internal target. The cryogenic Atomic Beam Source (ABS) [5] provides a polarized deuterium gas jet with an intensity of up to 8×10^{16} atoms/s and a very high degree of tensor polarization – above 98% from extreme values ($+1$ or -2), while vector polarization was always zero. It takes less than a second to alternate the polarization. During the run the polarization settings were switched every 30 seconds to suppress systematic uncertainties. Polarization of the gas stored inside the cell is degraded due to various depolarizing processes. The target polarization was determined by a polarimeter based on a measurement of an asymmetry in elastic e-d scattering at a small transferred momentum ~ 1.6 fm^{-1} [6]. The polarimeter was operated simultaneously with the main detector. Tensor polarization averaged over the whole run of data taking was found to be $P_{zz}^{+} = 0.308 \pm 0.020 \pm 0.009$, where the first uncertainty is statistical and the second one is systematic. The latter uncertainty includes a spread of theoretical predictions for the analyzing power. We assume that depolarization processes inside the cell occur identically in both polarization states – see [7]. Therefore $P_{zz}^{-}/P_{zz}^{+} = -2$, i.e. the same as for the ABS beam.

In this experiment we measured the counting rate asymmetry for two signs of tensor polarization of the deuterium target in disintegration of the deuteron by a 2-GeV electron scattered

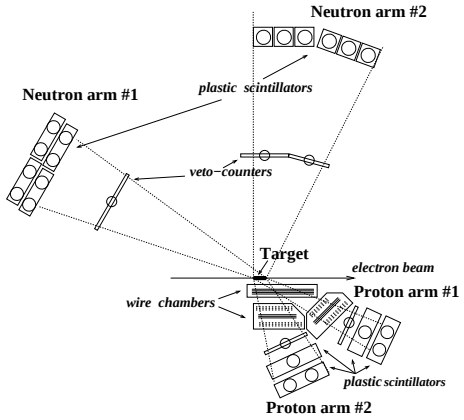

FIG. 1: Schematic side view of the particle detectors.

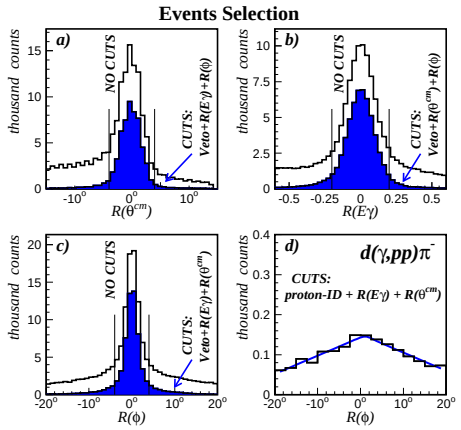

FIG. 2: Selection of two-body deuteron photodisintegration events. Panels a)–c) are histograms of correlation parameters: $R(\vartheta^{cm}) = \vartheta^{cm}_{(p)} - \vartheta^{cm}_{(n)} - \pi$, $R(E_\gamma) = (E^{(p)}_\gamma - E^{(n)}_\gamma)/((E^{(p)}_\gamma + E^{(n)}_\gamma)/2)$, $R(\varphi) = \varphi_p - \varphi_n - \pi$. Shaded histograms are for all cuts applied except the cut on the shown parameter. Vertical lines indicate the cut on the shown parameter. Panel d) shows a shape of out-of-plane events distribution for the three-body deuteron disintegration, which is selected by identifying a proton in the neutron arm using TOF/E and ΔE/E analysis.

forward, i.e. at an angle $\vartheta_e = 0^\circ$. In final state we detect the proton and neutron in coincidence, the scattered electron is not detected. Scattering of an electron at 0° is equivalent to the radiation of a real photon, which is then absorbed by a deuteron – that is why in such a set-up it is the *photo*–disintegration, that is studied.

The experimental tensor target asymmetry is defined as

$$a^T = \sqrt{2}\frac{N^+ - N^-}{P^+_{zz}N^- - P^-_{zz}N^+}, \qquad (2)$$

where N^+ (N^-) denotes the number of events detected with positive (negative) target polarization.

In order to disentangle the three components of tensor analyzing power we collected data for three settings of the magnetic field, defining the polarization axis: $\theta_{\rm H0} = 0^\circ$, $\theta_{\rm H1} = 54.7^\circ$ and $\theta_{\rm H2} = 125.3^\circ$, with ϕ_H close to 0° for all settings. According to Eq. 1 the target asymmetry in these cases is proportional to $a^T_0 \sim c_0{\rm T}_{20}$, $a^T_1 \sim (-c_1{\rm T}_{21} + c_2{\rm T}_{22})$ and $a^T_2 \sim (+c_1{\rm T}_{21} + c_2{\rm T}_{22})$ respectively. Here c_0, c_1, c_2 are constants defined by a geometry of detector and target. Therefore all three tensor moments are separated unambiguously.

The particle detector consists of two pairs of arms for detecting protons and neutrons in coincidence, as shown in Fig. 1. The first (second) pair covers an angle range of $\theta^{cm}_p = 24^\circ$ to 48° ($\theta^{cm}_p = 70^\circ$ to 102°). Each proton arm includes wire chambers for tracking and 3 layers of plastic scintillators ($2 + 12 + 12$cm thick). Neutron arms consist of plastic scintillators: 2-cm charged particle veto counters followed by 20-cm or $12 + 12$cm scintillator bars placed at a largest available distance from the target, about 3 m, for the best TOF measurement. Azimuthal angular acceptance was $\Delta\varphi = 20^\circ$ for all arms.

Particle identification was based on the veto signal and TOF analysis for neutrons and on TOF and ΔE/E analysis for protons. Further event selection relies on kinematic correlations characteristic of the two-body photodisintegration – see Fig 2*a–c*. One such property is a coplanarity of proton and neutron momenta ($|\phi_p - \phi_n| = \pi$). Assuming deuteron two-body disintegration by a photon emitted along the electron beam direction, one can reconstruct the photon energy and cm angles from the momentum vector of a single detected proton or neutron. This provides two more selection criteria: $E^{(p)}_\gamma = E^{(n)}_\gamma$ and $\vartheta^{cm}_{(p)} + \vartheta^{cm}_{(n)} = \pi$. Such cuts allow both to reject the background and to constrain the angle of γ-quantum emission close to 0°. An amount of inseparable residual background, which comes mostly from three-body photodisintegration $d(\gamma, pn)\pi^0$, was estimated from the analysis of a tail in the out-of-plane events distribution. The shape of the tail is determined by selecting the events of a similar 3-body disintegration process $d(\gamma, pp)\pi^-$ – see Fig 2*d*. After applying all cuts the fraction of unseparated background events was estimated to be from 1.5% (low E_γ region) to 5.6% (high E_γ region). The uncertainty from the unseparated background events is included in the statistical uncertainty.

The main source of systematic uncertainty is the uncertainty in the target polarization. The degree of polarization enters as a common factor for all data points. Other systematic uncertainties come from the inaccuracy of reconstruction of photon energy and proton CM–emission angle. Contribution of these parameters dominates at small photon energy where tensor analyzing powers change fast with energy. The false asymmetry is negligible because the period of reversing of polarization was very short (30 seconds) comparing to characteristic time of drift of any other experimental parameters, such as electron beam lifetime, target density variations, PMT gain instability, *etc*. Moreover, the beam current integral and time spent in each polarization state were measured precisely and taken into account in the analysis.

A list of contributions to the systematic error and their values for several data bins are shown in Table I. In Figures 4,5 systematic errors are presented as shaded bands at top or bottom of the plots.

TABLE I: Systematic errors for two data bins.

E_γ–bin	$45-70$ MeV			$140-180$ MeV		
θ_p^{cm}–bin	$78^\circ-102^\circ$			$74^\circ-102^\circ$		
	T_{20}	T_{21}	T_{22}	T_{20}	T_{21}	T_{22}
E_γ reconstruction	0.020	0.002	0.043	0.005	0.001	0.009
θ_p^{cm} reconstruction	0.001	0.010	0.001	0.003	0.015	0.005
Target polarization	0.021	0.003	0.035	0.049	0.010	0.080
Polarization orientation	0.001	0.010	0.001	0.002	0.024	0.003
Total	0.030	0.015	0.055	0.050	0.030	0.081

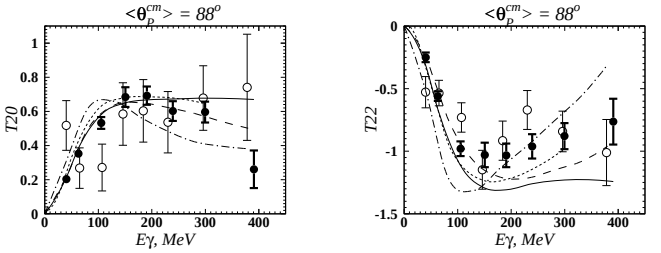

FIG. 3: Comparison of previous data [4] (open circles) and this work (filled circles). Only the part of the new data which corresponds to the kinematic conditions of the previous measurement is shown. Theoretical curves are the full calculation from [8] (solid line), the full calculation from [12] (dotted line), dashed and dash-dotted calculations from [13] with cutoff parameter $\Lambda = 1.2$ GeV/c (dashed line) and $\Lambda = 4m_\pi$ (dashed-dotted line).

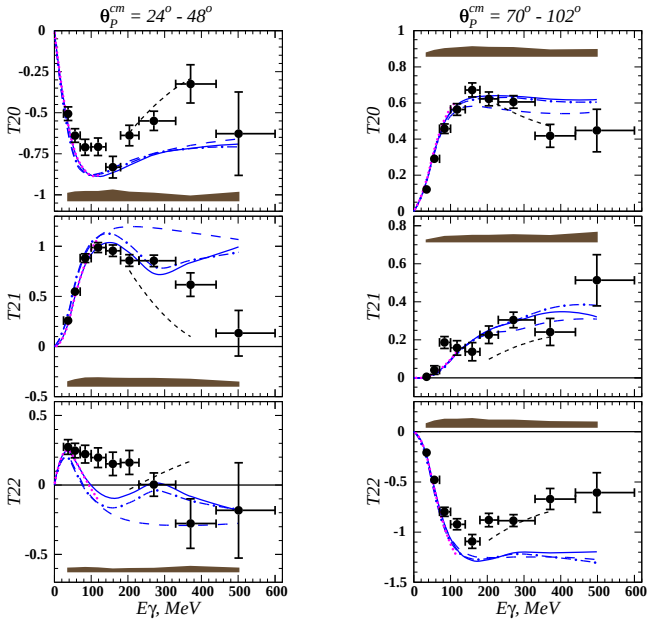

FIG. 4: (color online). Tensor analyzing powers vs. photon energy. Vertical bars are statistical uncertainties; horizontal bars indicate the bin size. Shaded bands show systematic uncertainties. Theoretical predictions are from Arenhövel [8] "N+MEC" (blue long-dashed line), "N+MEC+IC" (blue dash-dotted line), and "N+MEC+IC+RC" (solid line) models, from Levchuk [9] (magenta dotted line), and from Schwamb [11] (black short-dashed line).

Tensor analyzing powers are functions of two variables, and usually E_γ^{lab} and ϑ_p^{cm} are chosen. Our data cover substantially broad continuous regions of both variables. Binning of the experimental data was done in order to provide both sufficient statistical precision and a reasonable number of bins to display the dependence of tensor moments on kinematic variables.

To compare the new data with the results of earlier measurements [4], a subset of the data, where the kinematic acceptances of two measurements overlap, was selected – see Fig. 3 [15]. One can see that two measurements are consistent within uncertainties.

To compare the data to theoretical predictions we have performed an event weighted averaging of the theory over the phase-space of each experimental bin. The calculation [8] starts from a one-body current using the Bonn OBEPR NN potential with the major part of meson exchange currents (MEC) included implicitly via the Siegert operators; this model is denoted as "normal" (N). Then explicit pion exchange currents ("+MEC"), isobar configurations ("+IC") and the leading order relativistic corrections ("+RC") are added successively. The calculation of [9] was done in a diagrammatic approach with all MEC, including heavy-meson ones, introduced explicitly, and isobar configurations and relativistic corrections added. This calculation is restricted to the photon energy below pion production threshold. In [10] the deuteron photodisintegration beyond pion production threshold is studied in a coupled–channel approach including $N\Delta$ and πd channels, with the dynamical treatment of the pion. In consequence the NN potential and π–MEC become retarded and electromagnetic loop corrections have been incorporated. In [11] this concept was further elaborated and numerical results for various observables were obtained.

The dependence of tensor analyzing powers on photon energy is plotted in Fig. 4. Here the whole dataset is divided into two θ_p^{cm} bins, each related to the data from one pair of detector arms. Alternately, in Fig 5 the tensor moments versus θ_p^{cm} are shown for eight E_γ-bins. The numerical results are available from [14].

Figures 4 and 5 show that up to about pion production threshold, there is little variation between the theoretical calculations [8, 9], and there is good agreement between these calculations and the data. The most noticeable difference is that T_{22} tends to be slightly more positive than calculated.

Above pion production, the calculations become significantly more complex due to the larger effects of relativity and the increasing importance of additional channels, as the pion can propagate on-shell, and the energy approaches the Δ resonance region. We see greater variations between the older calculation of [8] and the more modern calculation of [11]. The more modern calculations improve the description of T_{20} and T_{22}, but do worse for T_{21}. Despite the disagreement in details, it is clear that there is a good overall qualitative description of the polarization data, which is a difficult test for theory. As both calculations are grounded in fits to nucleon-nucleon and meson photoproduction data, one would hope that the refinements in theory over time and the improvements in the description of the underlying reactions would lead to a clear improvement in all the deuteron photodisintegration data, but this is not the case. The pattern of agreement between theory

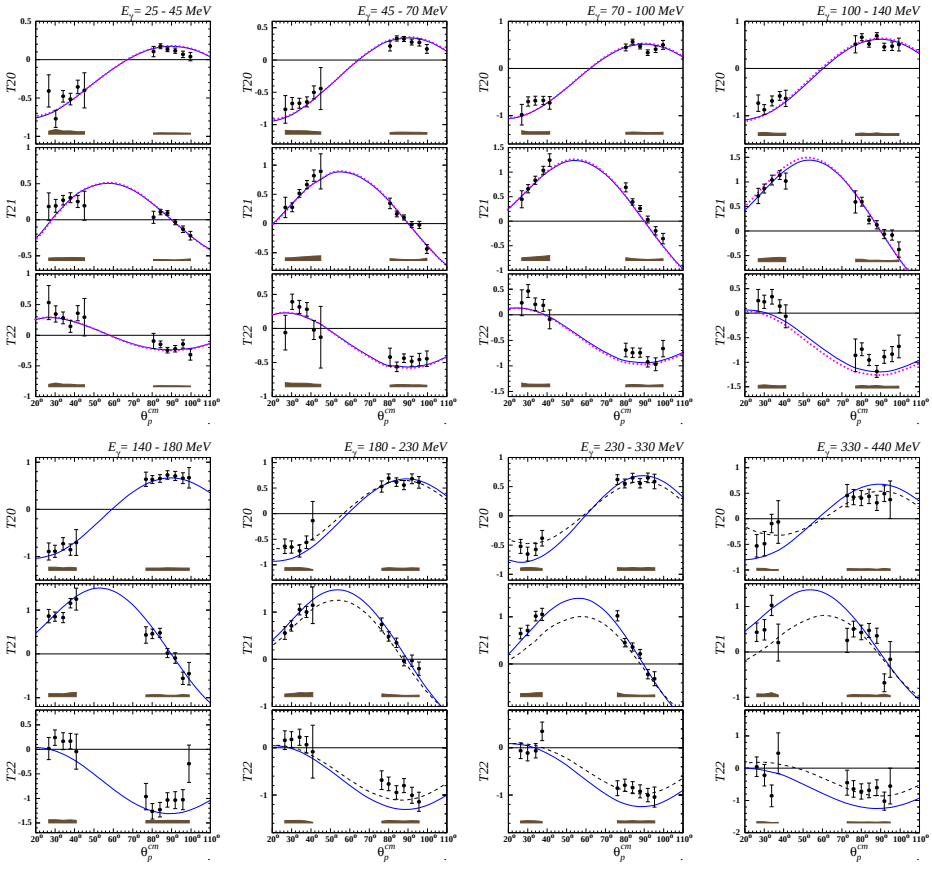

FIG. 5: (color online) Tensor analyzing powers vs. proton emission angle for eight E_γ-bins. Each θ_p^{cm} bin is 4° wide. See Fig.4 for notation.

and experiment is similar to that seen for other polarization observables such as p_y and Σ; the quality of the agreement decreases at higher energies.

In summary, a new measurement of tensor analyzing powers T_{20}, T_{21} and T_{22} in deuteron photodisintegration, substantially enhancing the quality and kinematic span of the existing experimental data, has been performed. Theoretical calculations provide an excellent description of these polarization data below pion production threshold, and a very good description above pion production threshold. The remaining discrepancies could reflect the theoretical uncertainties or some missing or poorly modeled underlying dynamics.

We gratefully acknowledge the staff of VEPP–3 accelerator facility for excellent performance of the ring during the data taking. We are grateful to H.Arenhövel, M.Levchuk and M.Schwamb for useful discussions and for providing us with the results of their calculations. This work was supported in part by Russian Foundation for Basic Research, grants 01-02-16929, 04-02-16434, 05-02-17080 and 05-02-17688, the U.S. Department of Energy, Office of Nuclear Physics, under contract no. W-31-109-ENG-38, and the U.S. National Science Foundation, grant PHY-03-54871.

[1] R. Gilman and F. Gross, J. Phys. **G28**, R37 (2002).
[2] M.V. Mostovoy, *et al.*, Phys. Lett. **B189**, 181 (1987).
[3] K.H.Althoff *et al.*, Z Phys. **C43**, 375 (1989).
[4] S.I. Mishnev, *et al.*, Phys. Lett. **B302**, 23 (1993).
[5] M.V. Dyug *et al.*, Nucl. Instrum. Methods **A495**, 8 (2002).
[6] M.V. Dyug *et.al.*, Nucl. Instrum. Methods **A536**, 344 (2005).
[7] M. Ferro-Luzzi *et al.*, Phys. Rev. Lett. **77**, 2630 (1996).
[8] K.-M. Schmitt and H. Arenhövel, Few-Body Syst. 7, 95 (1989), H.Arenhövel and M. Sanzone, Few-Body Syst. Suppl. 3, 1 (1991), F. Ritz, H. Arenhövel, and T. Wilbois, Few-Body Syst. 24, 123 (1998)
[9] M.I. Levchuk, Few-Body Syst. **19**, 77 (1995) and private communication.
[10] M. Schwamb, H. Arenhövel, Nucl. Phys. **A 690**, 647 (2001), and Nucl. Phys. **A 696**, 556 (2001)
[11] M. Schwamb, habilitation thesis, Johannes Gutenberg-Universität at Mainz, 2006
[12] M.I. Levchuk, Minsk Inst. Phys., preprint **N 609** (1990).
[13] Yu.P. Mel'nik and A.V. Shebeko, Phys. Rev. **C48**, 23 (1993).
[14] http://www.inp.nsk.su/∼rachek/photodisintegration.html
[15] Note that the data from [4] were corrected by re-analysis of the target polarimeter data, resulting in a target polarization $P_{zz} = 0.48$ instead of $P_{zz} = 0.58$ used in [4].